

See discussions, stats, and author profiles for this publication at: <https://www.researchgate.net/publication/265297292>

Introducing Mutations to Modify the C13/C9 Ratio in Linoleic Acid Oxygenations Catalyzed by Rabbit 15-Lipoxygenase: A QM/MM and MD Study

ARTICLE in CHEMPHYSICHEM · SEPTEMBER 2014

Impact Factor: 3.42 · DOI: 10.1002/cphc.201402471

CITATION

1

READS

22

4 AUTHORS:



Reynier Suardiaz

King's College London

33 PUBLICATIONS 175 CITATIONS

SEE PROFILE



Laura Masgrau

Autonomous University of Barcelona

41 PUBLICATIONS 727 CITATIONS

SEE PROFILE



José M Lluch

Autonomous University of Barcelona

270 PUBLICATIONS 4,266 CITATIONS

SEE PROFILE



Angels Gonzalez-Lafont

Autonomous University of Barcelona

119 PUBLICATIONS 1,992 CITATIONS

SEE PROFILE

Introducing Mutations to Modify the C13/C9 Ratio in Linoleic Acid Oxygenations Catalyzed by Rabbit 15-Lipoxygenase: A QM/MM and MD Study**

Reynier Suardíaz,^[a, b] Laura Masgrau,^[b] José M. Lluch,^[a, b] and Àngels González-Lafont^{*,[a, b]}

Lipoxygenases (LOs) are a family of nonheme iron-containing enzymes that catalyze the hydroperoxidation of several polyunsaturated fatty acids with a huge regio- and stereospecificity. Mammalian 15-LO-1 yields almost exclusively oxygenation at the C13 position of the linoleic acid (LA), its preferred substrate. This is very important because metabolites derived from oxidation in distinct positions produce opposite physiological effects. We have combined here quantum mechanics/molecular mechanics calculations with molecular dynamics simula-

tions to show how a suitable mutation of the rabbit 15-LO-1 enzyme can produce a significant amount of products derived from oxygenation at the C9 position of LA. In effect, the Leu597Val or Leu597Ala mutants are predicted to lead to a diminution of the oxygenation C13/C9 ratio in LA as huge as five orders of magnitude. This shows that the conserved residue Leu597 actually drives the regiospecific hydroperoxidation of LA catalyzed by 15-LO-1 enzyme.

1. Introduction

Enzymes sustain life, allowing cells to carry out chemical reactions very quickly. Moreover, they are usually very regio- and stereospecific. This very important feature makes possible the formation of the unique product required in each case with a high yield and without the appearance of any unwished, side reactions. Shedding light on the way each enzyme manages to achieve its specificity is the key for understanding how it works and for designing a modified enzyme with a different function.^[1]

Particularly interesting are lipoxygenases (LOs), a family of nonheme iron-containing enzymes that catalyze the hydroperoxidation of several polyunsaturated fatty acids (PUFAs), as linoleic acid (LA, 18:2, *n*–6), arachidonic acid (AA, 20:4, *n*–6), eicosapentaenoic acid (EPA, 20:5, *n*–3) and docosahexaenoic acid (DHA, 22:6, *n*–3).^[2–6] The specificity of LOs in mammals is so important that they are classified with respect to their position of dioxygenation of AA (5-, 8-, 12, and 15-LOs).^[7–11]

The whole hydroperoxidation reaction begins (see Scheme 1S in the Supporting Information) with the pro-S hydrogen abstraction from a bisallylic carbon atom of the PUFA

by the Fe^{III}–OH[–] cofactor of the LO in its active form, giving a pentadienyl π radical in the PUFA and Fe^{II}–H₂O in the LO. Subsequent addition of molecular oxygen from the opposite side of the radical plane (antarafacial reaction) to a carbon-centered substrate radical forms a peroxy radical that is finally reduced to the hydroperoxy product by hydrogen transfer from the Fe^{II}–H₂O moiety.^[4, 11]


Some conserved bulky hydrophobic residues in the lipoxygenase family have been considered to be mostly responsible for the specificity of the global reaction. Thus, results obtained by Knapp et al.^[12] by means of steady-state kinetics and product distribution data from single-point mutants of soybean lipoxygenase-1 (SLO-1) indicate that Leu546 and Leu754 granted selectivity for 13-(S)-hydroperoxyoctadecadienoic acid (13-(S)-HPODE) by sterically blocking O₂ access to the C9 position of LA. So, the prevailing product for wild-type SLO-1 was 13-(S)-HPODE (95%), appearing trace amounts of 13-(R) (3%), 9-(S) (<1%), and 9-(R) (2%) isomers. However, the Leu754Ala mutant reduces the overall catalysis yielding a quite remarkable decrease of the still dominant 13-(S) isomer (62%), and a concomitant augment not only of the 9-(R) isomer (16%), but also of the 13-(R) (12%) and 9-(S) (10%) products.

To the best of our knowledge, experimental results corresponding to the same mutation for other members of the lipoxygenase family have not been published so far. However, we have recently^[13, 14] combined quantum mechanics/molecular mechanics (QM/MM) electronic structure calculations with molecular dynamics (MD) simulations to show that the oxygenation of LA at C9 catalyzed by rabbit 15-LO-1 (15-rLO) is hindered by two steric-shielding residues, Leu597 (the residue in 15-rLO corresponding to Leu754 in SLO-1) and Gln548. This finding is especially relevant because LA is the preferred substrate of 15-LOX-1,^[15] yielding—almost exclusively—oxidation

[a] Dr. R. Suardíaz, Prof. Dr. J. M. Lluch, Prof. Dr. À. González-Lafont
Departament de Química
Universitat Autònoma de Barcelona
Bellaterra 08193, Barcelona (Spain)
E-mail: Angels.Gonzalez@uab.cat

[b] Dr. R. Suardíaz, Dr. L. Masgrau, Prof. Dr. J. M. Lluch,
Prof. Dr. À. González-Lafont
Institut de Biotecnologia i de Biomedicina (IBB)
Universitat Autònoma de Barcelona
Bellaterra 08193, Barcelona (Spain)

[**] QM=quantum mechanics, MM=molecular mechanics, and MD=molecular dynamic.

 Supporting Information for this article is available on the WWW under <http://dx.doi.org/10.1002/cphc.201402471>.

at the C13 position,^[16,17] LA is the most abundant (40–45%) PUFA in atherosclerotic plaques,^[18] and 13-hydroxyoctadecadienoic acid (13-HODE, coming from 13-HPODE through a quick reduction) enhances protective mechanisms in early lesions, while 9-hydroxyoctadecadienoic acid (9-HODE, generated from 9-HPODE) has harmful, pro-inflammatory effects contributing to lesion progression.^[18] On the other hand, we have already applied^[19,20] theoretical methods to show that the steric shielding of several residues, mainly Leu597, causes the predominant oxygenation at C15 of AA (in front of C11) catalyzed by 15-rLO.

The X-ray structure of human 15-LO-1 (15-hLO) has not been reported yet. However, 15-rLO has approximately 80% sequence identity with 15-hLO,^[21] and its crystallographic structure is available (Protein Data Bank entry 2P0M; resolution 2.4 Å).^[22] Then, in this paper we intend to design mutants of 15-rLO with an “in silico” oxygenation C13/C9 ratio in LA significantly altered with respect to the wild-type enzyme. In particular, we have shortened the two residues that seem to hinder by steric-shielding the oxygenation at the position C9 of LA. We have tested the regiospecificity of the Leu597Val, Leu597Ala, and Gln548Asn mutants (see Figure 1S). To this purpose, we have combined QM/MM electronic-structure calculations with MD simulations to study the addition of molecular oxygen to the pentadienyl radical of LA (after the hydrogen abstraction from C11 of LA) in a model including the whole LA and the entire 15-rLO enzyme conveniently solvated. We think that our results can contribute to learn how the regiospecificity of enzymes can be governed as needed.

Computational Methods

Starting Geometries

Starting geometries have been taken from a previous work^[13] where prereactive minima, based on initial modeling of the 15rLO:LA complex by protein–ligand docking and molecular dynamics simulations,^[23] and reaction profiles were obtained for the molecular oxygen addition to C13 and C9 of the LA-pentadienyl radical (after hydrogen abstraction from C11) in wild-type 15rLO. One of those prereactive minima for the reaction of peroxidation was selected and the molecular oxygen was deleted. Residue Leu597 of these systems was mutated to Val or Ala, and residue Gln548 was mutated to Asn using the VMD software.^[24] After that, the substrate, all protein residues, and water molecules within 15 Å of the C11 of LA (2163 atoms for Leu597Val, 2115 for Leu597Ala, and 2156 for Gln548Asn), were submitted to a first optimization at the QM(B3LYP)/MM level in conjunction with the 6-31G(d) basis set, except for Fe for which LANL2DZ was employed. The rest of the atoms in the system were kept frozen. The QM# region (atoms in bold in Figure 1, except for the O₂ molecule) consisted of 62 atoms (link atoms not included). For each mutant, the system was then submitted to 50 ps of QM(OM3)/MM-MD^[25] simulation to generate a number of structures according to a Boltzmann distribution at 300 K (in the Supporting Information, it is shown that the time of the simulation is long enough). To save computer time, the QM region for the QM/MM-MDs included only the part of the LA depicted in bold in Figure 1, which was treated at the semiempirical level with the OM3 Hamiltonian.^[25] MD trajectories were subjected to a clustering process using the root-mean-square deviation as

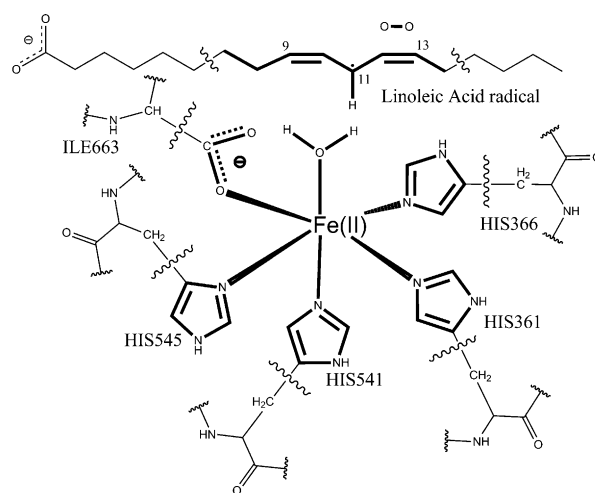


Figure 1. Schematic view showing the QM/MM partition used in this work. The QM atoms (with the biggest QM region: 64 atoms) are depicted in bold. The boundary between the QM and MM regions is indicated by wavy lines.

a distance function, a distance cutoff of 0.1 Å and without weighting, as implemented in VMD. In the three cases, there was a predominant cluster with more than 90% of the geometries. For each mutant, a representative geometry was selected from this cluster so that it was as close as possible to the average geometry of the cluster (the average geometry being a hypothetical structure with the shortest average distance to the other constituents of the cluster).

QM/MM Calculations

QM/MM electronic-structure calculations were carried out with the modular package Chemshell^[26] using TURBOMOLE^[27] for all the density functional theory (DFT) calculations, and MNDO99^[28] for the semiempirical ones. The MM part was treated in all cases with the CHARMM22^[29,30] and CHARMM27^[31,32] (for the moiety of LA included in the MM region) force fields through the DL_POLY^[33] module in Chemshell. Ad hoc parameters for the simulation of the Fe^{II} coordination system (when included in the MM part) were used. An electronic embedding scheme^[34] was adopted in all the calculations and hydrogen link atoms were used to treat the QM/MM boundary with the charge shift model.^[35] No cutoffs were introduced for the nonbonding MM and QM/MM interactions. After obtaining the QM(B3LYP)/MM potential energy profiles as a function of an appropriate reaction coordinate, the corresponding highest energy point of each profile was used as starting geometry to directly locate the transition state structure (TS). Frequency calculations on the QM region confirmed that all the located transition state structures are characterized by a single imaginary frequency (unless otherwise stated) and a suitable transition vector that corresponds to the investigated reaction. The QM/MM optimizations were carried out using the limited-memory Broyden–Fletcher–Goldfarb–Shanno (L-BFGS) algorithm^[36,37] in the case of energy minimizations, and the microiterative optimizer, combining both the partitioned rational function optimizer (P-RFO)^[38,39] and the L-BFGS, during the transition-state searches. All these algorithms are implemented in the HDLCopt module^[40] of Chemshell. In the QM/MM-MD simulations, the system was gradually heated from 10 to 300 K in 6 ps, equilibrated at 300 K for 3 ps and the production time was 50 ps. The bonds involving hydrogen atoms in the MM region were fixed by the SHAKE algorithm. We have taken

the NPA^[41] (natural population analysis) atomic populations evaluated from the spin density (SD) as implemented in TURBOMOLE.^[27]

2. Results and Discussion

2.1 Oxygen Positioning and Reaction Profiles

We have firstly determined the positions of the oxygen molecule prior to its attack to the LA-pentadienyl radical. For each mutant, the representative geometry chosen in the clustering process (see starting geometries above) was fully optimized at the QM(B3LYP)/MM level (again, the QM region is represented by the atoms in bold in Figure 1, except for the O₂ molecule). These optimized structures were then used to locate the corresponding prereactive minima for the peroxidation reaction in the following way: A semi-sphere of radius 2.5 Å, placed on the opposite side of the Fe^{II}–H₂O moiety with respect to the pentadienyl radical plane, and centered at each reactive carbon position (C9 or C13), was defined to be consistent with the antarafacial character of the reaction.^[11] O₂ molecules were homogeneously placed at distinct locations on each semi-sphere and pointing to the corresponding reactive carbon atom. The same procedure was repeated for spheres of radius 3.0, 3.5, and 4.0 Å. In all, 32 different positions of the O₂ molecule, homogeneously distributed around the reactive carbons of the LA-pentadienyl radical, were generated for each mutant. With the O₂ molecule added, the QM region now included all atoms depicted in bold in Figure 1 and consisted of 64 atoms (link atoms not included). The spin multiplicity of the system was taken as six. Partial geometry optimizations at the QM-(B3LYP)/MM level were performed for those 32 structures, which correspond to 32 different positions of one oxygen molecule around the reactive carbon. During those optimizations, the distance between the reactive carbon and the closest oxygen atom was kept frozen. From those partially optimized geometries, the most stable ones within a range of 10 kcal mol^{−1} were selected for each of the two sets (C9 or C13). Next, the selected structures were fully optimized. It is worth noting that several different geometries obtained after partial optimization collapsed to the same structure after full geometry optimization. The most stable structures within a range of 5 kcal mol^{−1} were selected this time for each set. After following this computational procedure to locate the most stable positions of the O₂ molecule around the fatty acid radical, five geometries with different O₂ orientations were obtained for the Leu597Val mutant, four for the Leu597Ala mutant, and six for the Gln548Asn mutant.

Those prereactive minima were used as starting points for the calculation of the potential energy profiles for the O₂ addition to the C13 or C9 atoms of the LA-pentadienyl radical. The reaction paths were scanned by performing constrained geometry optimizations along the reaction coordinate O–C(C13/C9) by steps of 0.1 Å. The QM region for all those geometry optimizations included all the 64 atoms depicted in bold in Figure 1, and it was described at the B3LYP/6-31G(d) level, except for Fe for which the LANL2DZ basis set was used.

In all, the system now includes 11 770, 11 761, or 11 785 atoms, with 2163, 2115, or 2156 of them being mobile, for the Leu597Val, Leu597Ala or Gln548Asn mutants, respectively. As done for the wild-type enzyme, NPA atomic populations evaluated from spin densities (SDs) on specific atoms were checked along the potential energy profiles. For all the mutants, the addition of molecular oxygen both to C13 or to C9, presents SDs on C13 or C9 that go from around −0.4 to 0.0 au each; the SDs on the oxygen atoms go from 1.0 to 0.6 or to 0.4 au (the latter corresponding to the oxygen atom closest to the reacting carbon atom) as the peroxide bond is formed. The SD on Fe^{II} remains unchanged (3.7 au) along the reaction coordinate (see Figure 2S). Similar results were obtained for the wild-type enzyme.^[13,14]

The calculated potential energy profiles provided starting geometries for subsequent direct localization of the transition-state structures. From here on, unless otherwise indicated, all the potential energy barriers indicated in the text and the table correspond to fully characterized transition-state structures.

2.2 The Leu597Val Mutant

Five prereactive minima were found for this mutant: four of them with the oxygen positioned ready to react at C13 and one at C9 (see Table 1). The potential energy barriers for the four transition states corresponding to the addition to C13 range from 4.30 to 5.59 kcal mol^{−1}, while the unique transition state for the addition to C9 involves 5.60 kcal mol^{−1}. According to these results, the regiospecificity of this reaction should be qualitatively the same as in the wild-type enzyme, that is, more products with O₂ addition on position C13 than on C9. However, the C13/C9 proportion has undergone an extremely drastic change. In effect, in the case of the wild-type enzyme,^[13] the same kind of calculations yielded a barrier height of 2.33 kcal mol^{−1} for O₂ addition to C13, but as high as 11.27 kcal mol^{−1} for O₂ addition to C9. Assuming kinetic control for the regiospecificity^[9,11] and using conventional transition-state theory, if the difference in the calculated potential energy barriers is considered to be an acceptable measure of the difference between the corresponding phenomenological free energy barriers, we can predict a C13/C9 ratio greater than 10⁶ for the wild-type 15-rLO, what justifies the fact that the experimental oxidation occurs almost exclusively at the C13 position of LA. Very interestingly, as for the Leu597Val mutant, just comparing the lowest potential energy barrier height for the reaction at C13 with the one corresponding to the reaction at C9, our theoretical prediction is a C13/C9 ratio of nine, with a reduction of the regiospecificity as huge as five orders of magnitude. This impressive change confirms the very important role of the bulky hydrophobic residue Leu597, driving the regiospecific hydroperoxidation of LA catalyzed by 15-rLO, and shows that there is a wide margin of artificial modification of the specificity of enzymes.

On the other hand, the reaction in the Leu597Val mutant keeps the same *S* stereospecificity as in the wild-type enzyme. As described in a previous work, the residue Leu597 shields C9

Table 1. Prereactive minima for O₂ addition to the LA-pentadienyl radical located for the three mutants: Initial distance from the oxygen atom closest to the reacting carbon atom, the same distance at the transition state of the corresponding addition, and potential energy barrier for each case. All the located transition states have a clear single imaginary frequency, except for the three corresponding to the addition to C9 in the Gln548Asn mutant (see text).

Mutant	Reactive position	Minimum	O–C distance (minimum) [Å]	O–C distance (TS) [Å]	Potential energy barrier [kcal mol ⁻¹]
Leu597Val	C13	1	3.37	2.16	4.30
		2	3.34	2.18	5.16
		3	3.50	2.14	5.38
		4	4.45	2.14	5.59
Leu597Ala	C9	1	5.13	2.15	5.60
	C13	1	3.60	2.14	3.78
	C9	1	4.13	2.18	5.31
	C9	2	It converges to minimum 3		
Gln548Asn	C13	3	4.62	2.18	7.01
	C13	1	3.20	2.41	2.71
	C13	2	3.89	2.20	5.84
	C13	3	3.15	2.25	2.06
	C9	1	4.16	2.26	10.21
	C9	2	4.05	2.26	10.10
	C9	3	4.14	2.24	12.20
	C9				

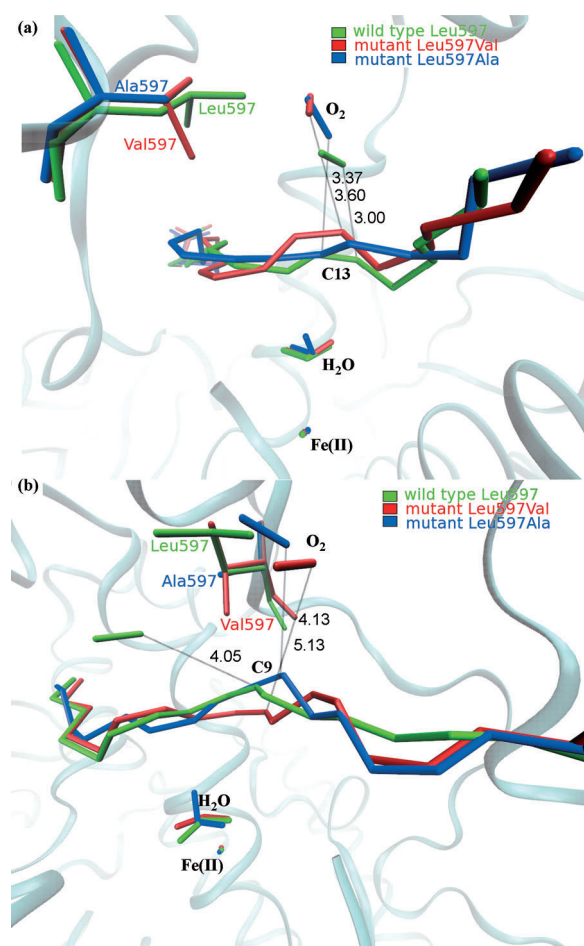
in the wild-type enzyme and, consequently, hinders O₂ addition at this position. The mutation by a residue with a shorter side chain, such as Val, creates some extra space where the O₂ molecule can accommodate to form a prereactive minimum for addition on C9, but LA keeps its average position inside the enzyme's active site, as can be seen after the corresponding QM/MM geometry optimizations and QM/MM-MD simulations. The relative positions of the LA-pentadienyl radical and O₂ inside the Leu597Val mutant and inside the wild-type enzyme are depicted in Figure 2 for the respective prereactive minima that are associated to the lowest potential energy barrier in each case. Notice that in the case of the oxidation addition at C9 (Figure 2b), the O₂ molecule occupies a position in the mutants that is occupied by the Leu597 in the wild-type enzyme.

2.3 The Leu597Ala Mutant

This time the mutation involves a shorter residue (Ala), but the results are qualitatively the same (see Table 1 and Figure 2). Four prereactive minima were found for this mutant. One of them has the oxygen positioned ready to react at C13, with a potential energy barrier of 3.78 kcal mol⁻¹. The other three prereactive minima correspond to addition to C9. When calculating the potential energy profile, the second of them converged to the third. So, the two potential energy barriers for the molecular oxygen addition to C9 turn out to be 5.31 and 7.01 kcal mol⁻¹. This way the C13/C9 ratio (now 12) for the Leu597Ala mutant is quite similar to the one corresponding to the Leu597Val mutant. The decisive role of Leu597 in determining the regioselectivity of the hydroperoxidation of LA catalyzed by 15-rLO is again confirmed. The same S stereospecificity as in the wild-type enzyme is conserved, as explained above.

2.4 The Gln548Asn Mutant

For this mutant we found three prereactive minima for the reaction at C13 and the same number for reaction at C9 (see Table 1). The potential energy barriers for the three transition states corresponding to the addition to C13 range from 2.06 to 5.84 kcal mol⁻¹, while the three transition states leading to the addition to C9 involve barriers between 10.10 and 10.21 kcal mol⁻¹. At this point we have to mention that those last three transition states were actually located using the microiterative optimizer, as described in the Computational Methods section. However, they are placed on

**Figure 2.** Prereactive minima for O₂ addition to C13 (a) and C9 (b) of the LA-pentadienyl radical inside the wild-type enzyme (green), the Leu597Val mutant (red), and the Leu597Ala mutant (blue). Only the prereactive minima that evolve with the lowest potential energy barriers in each case are pictured.

a quite flat region of the potential energy surfaces, in such a way that in each case, a very small real frequency, not imaginary, is obtained along the right reaction coordinate. Having said that, we can predict a C13/C9 ratio for the Gln584Asn mutant, taking the two respective lowest potential energy barriers, somewhat lower, but within the same order of magnitude, than for wild-type 15-rLO. That is, this mutation would not significantly alter the almost exclusively formation of products derived from oxygenation at C13 of LA. Gln548 plays a much less important role in the regiospecificity of this reaction than the residue Leu597. Figure 3 shows the relative positions of LA and O₂ in the prereactive minima that evolve with the lowest potential energy barriers. As can be seen, there is just a small change in the position of the LA due to the mutation, in such a way that the S stereospecificity is conserved in all cases.

At this point it is worth commenting that as the molecular oxygen approaches to the attacked carbon atom (C13 or C9), it becomes less and less free with the corresponding loss of entropy. However, this loss of entropy will be quite similar, independently of both the particular carbon atom where the addition happens and of the particular mutant that catalyzes the reaction. Then the entropy contribution would increase the barriers and convert exergonic additions in terms of potential energy in less exergonic reactions in terms of free energy, but it is expected to be roughly equivalent for the 14 potential energy profiles we have studied.^[42] As a consequence, we can assume that the relative comparison of the potential energy

barriers is enough in the present case to discuss the regiospecificity of the molecular oxygen addition.

3. Conclusions

We have combined QM/MM electronic-structure calculations with MD simulations to study the addition of molecular oxygen to the pentadienyl radical of linoleic acid (after the hydrogen abstraction from C11 of LA), catalyzed by several mutants of the rabbit 15-LO-1 enzyme. To obtain reliable results, in spite of the size of the systems (almost 12000 atoms), we applied density functional theory to describe the QM region and included in the "in silico" model the complete enzymes, conveniently solvated, and the entire LA. Since 15-rLO almost exclusively yields oxidation at the C13 position,^[16,17] we investigated three mutants (namely, Leu597Val, Leu597Ala, and Gln548Asn), trying to get a 15-rLO mutant with an oxygenation C13/C9 ratio in LA significantly altered with respect to the wild-type enzyme. Leu597 and Gln548 are two residues that seem to hinder, by steric shielding, the oxygenation at the C9 position of LA.

After having calculated 14 potential energy profiles and directly located the corresponding transition states by using a microiterative optimizer, we can conclude that Leu597 actually drives the regiospecific hydroperoxidation of LA catalyzed by 15-rLO. When this bulky hydrophobic residue is shortened in the Leu597Val or Leu597Ala mutants, the oxygenation C13/C9 ratio in LA undergoes a diminution (and as a consequence, a decrease in regiospecificity) as huge as five orders of magnitude with respect to the wild-type enzyme, in such a way that a C13/C9 ratio of about ten is obtained in the mutant enzymes. That is, in contrast to wild-type 15-rLO, a significant amount of products derived from oxygenation at the C9 position of LA is predicted when the hydroperoxidation is catalyzed by the Leu597Val or Leu597Ala 15-rLO mutants. However, we predict an oxygenation C13/C9 ratio for the Gln584Asn mutant somewhat lower, but within the same order of magnitude, than for wild-type 15-rLO. That is, this mutation would not significantly alter the almost exclusively formation of products derived from oxygenation at C13 of LA. Gln548 plays a much less important role in the regiospecificity of this reaction than the residue Leu597. In all cases, the S stereospecificity is conserved.

We hope that our results can stimulate new experiments trying to govern the regiospecificity of the 15-LO-1 enzyme and, since Leu597 is a conserved residue in the family of these enzymes, of the rest of lipoxygenases.

Acknowledgements

We thank the Spanish Ministerio de Economía y Competitividad (Grant CTQ2011-24292) and the Generalitat de Catalunya (2009SGR409) for financial support. R.S. thanks the Alianza 4U program. We also acknowledge CESCA for computational facilities.

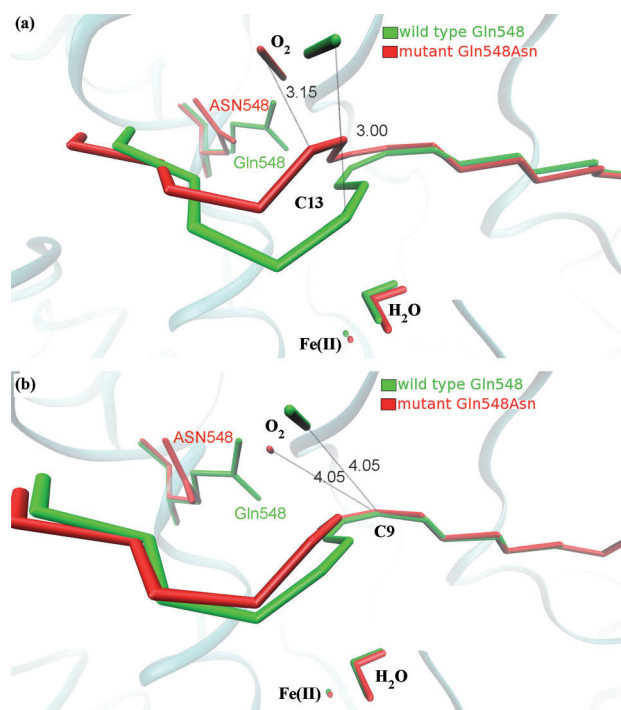


Figure 3. Prereactive minima for O₂ addition to C13 (a) and C9 (b) of the LA-pentadienyl radical inside the wild-type enzyme (green) and the Gln548Asn mutant (red). Only the prereactive minima that evolve with the lowest potential energy barriers in each case are pictured.

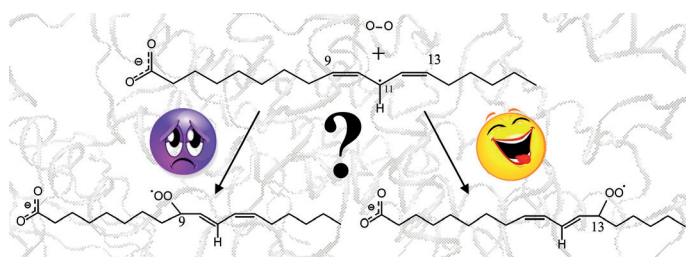
Keywords: computational chemistry • linoleic acid • 15-lipoxygenases • mutants • QM/MM calculations

- [1] D. Voet, J. G. Voet, *Biochemistry*, 4edth ed Wiley, Hoboken, **2004**.
- [2] A. D. Dobrian, D. C. Lieb, B. K. Cole, D. A. Taylor-Fishwick, S. K. Chakrabarti, J. L. Nadler, *Prog. Lipid Res.* **2011**, *50*, 115–131.
- [3] A. Catalano, A. Procopio, *Histol. Histopathol.* **2005**, *20*, 969–975.
- [4] J. Z. Haeggström, C. D. Funk, *Chem. Rev.* **2011**, *111*, 5866–5898.
- [5] Y.-C. Joo, D.-K. Oh, *Biotechnol. Adv.* **2012**, *30*, 1524–1532.
- [6] J. W. Phillis, L. A. Horrocks, A. A. Farooqui, *Brain Res. Rev.* **2006**, *52*, 201–243.
- [7] K. Schwarz, M. Walther, M. Anton, C. Gerth, I. Feussner, H. Kuhn, *J. Biol. Chem.* **2001**, *276*, 773–779.
- [8] G. Coffa, A. R. Brash, *Proc. Natl. Acad. Sci. USA* **2004**, *101*, 15579–15584.
- [9] C. Schneider, D. A. Pratt, N. A. Porter, A. R. Brash, *Chem. Biol.* **2007**, *14*, 473–488.
- [10] R. Vogel, C. Jansen, J. Roffeis, P. Reddanna, P. Forsell, H.-E. Claesson, H. Kühn, M. Walther, *J. Biol. Chem.* **2010**, *285*, 5369–5376.
- [11] I. Ivanov, D. Heydeck, K. Hofheinz, J. Roffeis, V. B. O'Donnell, H. Kühn, M. Walther, *Arch. Biochem. Biophys.* **2010**, *503*, 161–174.
- [12] M. J. Knapp, F. P. Seebeck, J. P. Klinman, *J. Am. Chem. Soc.* **2001**, *123*, 2931–2932.
- [13] R. Suardiaz, L. Masgrau, J. M. Lluch, À. González-Lafont, *J. Phys. Chem. B* **2013**, *117*, 3747–3754.
- [14] R. Suardiaz, L. Masgrau, À. González-Lafont, J. M. Lluch, *FEBS J.* **2013**, *280* (Suppl. 1), 94–94.
- [15] J. T. O'Flaherty, Y. Hu, R. E. Wooten, D. A. Horita, M. P. Samuel, M. J. Thomas, H. Sun, I. J. Edwards, *PLoS One* **2012**, *7*, e45480.
- [16] H. Kühn, J. Belkner, S. Zaiss, T. Fahrenklemper, S. Wohlfeil, *J. Exp. Med.* **1994**, *179*, 1903–1911.
- [17] K. Jostarndt, N. Gellert, T. Rubic, C. Weber, H. Kühn, B. Johansen, N. Hrboticky, J. Neuzil, *Biochem. Biophys. Res. Commun.* **2002**, *290*, 988–993.
- [18] V. Vangaveti, B. T. Baune, R. L. Kennedy, *Ther. Adv. Endocrinol. Metab.* **2010**, *1*, 51–60.
- [19] R. Suardiaz, L. Masgrau, J. M. Lluch, À. González-Lafont, *ChemPhysChem* **2013**, *14*, 3777–3787.
- [20] R. Suardiaz, L. Masgrau, J. M. Lluch, À. González-Lafont, *ChemPhysChem* **2014**, *15*, 2303–2310.
- [21] G. Rai, V. Kenyon, A. Jadhav, L. Schultz, M. Armstrong, J. B. Jameson, E. Hoobler, W. Leister, A. Simeonov, T. R. Holman, D. J. Maloney, *J. Med. Chem.* **2010**, *53*, 7392–7404.
- [22] J. Choi, J. K. Chon, S. Kim, W. Shin, *Proteins Struct. Funct. Bioinf.* **2008**, *70*, 1023–1032.
- [23] L. Toledo, L. Masgrau, J. M. Lluch, À. González-Lafont, *J. Comput.-Aided Mol. Des.* **2011**, *25*, 825–835.
- [24] W. Humphrey, A. Dalke, K. Schulten, *J. Molec. Graphics* **1996**, *14*, 33–38.
- [25] M. Korth, W. Thiel, *J. Chem. Theory Comput.* **2011**, *7*, 2929–2936.
- [26] P. Sherwood, A. H. de Vries, M. F. Guest, G. Schreckenbach, C. R. A. Catlow, S. A. French, A. A. Sokol, S. T. Bromley, W. Thiel, A. J. Turner, S. Billeter, F. Terstegen, S. Thiel, J. Kendrick, S. C. Rogers, J. Casci, M. Watson, F. King, E. Karlsen, M. Sjøvoll, A. Fahmi, A. Schäfer, C. Lennartz, *THEOCHEM* **2003**, *632*, 1–28.
- [27] R. Ahlrichs, M. Bär, M. Häser, H. Horn, C. Kölmel, *Chem. Phys. Lett.* **1989**, *162*, 165–169.
- [28] W. Thiel, MNDO99 program, version 7.0, Max-Planck-Institut für Kohlenforschung, Mülheim, Germany, **2005**.
- [29] A. D. MacKerell, D. Bashford, M. Bellott, R. L. Dunbrack, J. D. Evanseck, M. J. Field, S. Fischer, J. Gao, H. Guo, S. Ha, D. Joseph-McCarthy, L. Kuchnir, K. Kucera, F. T. K. Lau, C. Mattos, S. Michnick, T. Ngo, D. T. Nguyen, B. Prodhom, W. E. Reiher, B. Roux, M. Schlenkrich, J. C. Smith, R. Stote, J. Straub, M. Watanabe, J. Wiorkiewicz-Kuczera, D. Yin, M. Karplus, *J. Phys. Chem. B* **1998**, *102*, 3586–3616.
- [30] A. D. MacKerell, M. Feig, C. L. Brooks, *J. Comput. Chem.* **2004**, *25*, 1400–1415.
- [31] S. E. Feller, K. Gawrisch, A. D. MacKerell, *J. Am. Chem. Soc.* **2002**, *124*, 318–326.
- [32] S. E. Feller, A. D. MacKerell, *J. Phys. Chem. B* **2000**, *104*, 7510–7515.
- [33] W. Smith, T. R. Forester, *J. Mol. Graphics* **1996**, *14*, 136–141.
- [34] D. Bakowies, W. Thiel, *J. Phys. Chem.* **1996**, *100*, 10580–10594.
- [35] A. H. de Vries, P. Sherwood, S. J. Collins, A. M. Rigby, M. Rigutto, G. J. Kramer, *J. Phys. Chem. B* **1999**, *103*, 6133–6141.
- [36] J. Nocedal, *Math. Comp.* **1980**, *35*, 773–782.
- [37] D. Liu, J. Nocedal, *Math. Program.* **1989**, *45*, 503–528.
- [38] A. Banerjee, N. Adams, J. Simons, R. Shepard, *J. Phys. Chem.* **1985**, *89*, 52–57.
- [39] J. Baker, *J. Comput. Chem.* **1986**, *7*, 385–395.
- [40] S. R. Billeter, A. J. Turner, W. Thiel, *Phys. Chem. Chem. Phys.* **2000**, *2*, 2177–2186.
- [41] A. E. Reed, R. B. Weinstock, F. Weinhold, *J. Chem. Phys.* **1985**, *83*, 735–746.
- [42] I. Tejero, À. González-Lafont, J. M. Lluch, L. A. Eriksson, *J. Phys. Chem. B* **2007**, *111*, 5684–5693.

Received: July 1, 2014

Revised: July 31, 2014

Published online on ■■■ ■■, 2014



Very specific! Quantum mechanics/molecular mechanics calculations combined with molecular dynamics simulations show how Leu597 drives the re-

giospecific hydroperoxidation of linoleic acid catalyzed by rabbit 15-LO-1 enzyme.

R. Suardíaz, L. Masgrau, J. M. Lluch, A. González-Lafont*

■■ - ■■

Introducing Mutations to Modify the C13/C9 Ratio in Linoleic Acid Oxygenations Catalyzed by Rabbit 15-Lipoxygenase: A QM/MM and MD Study

